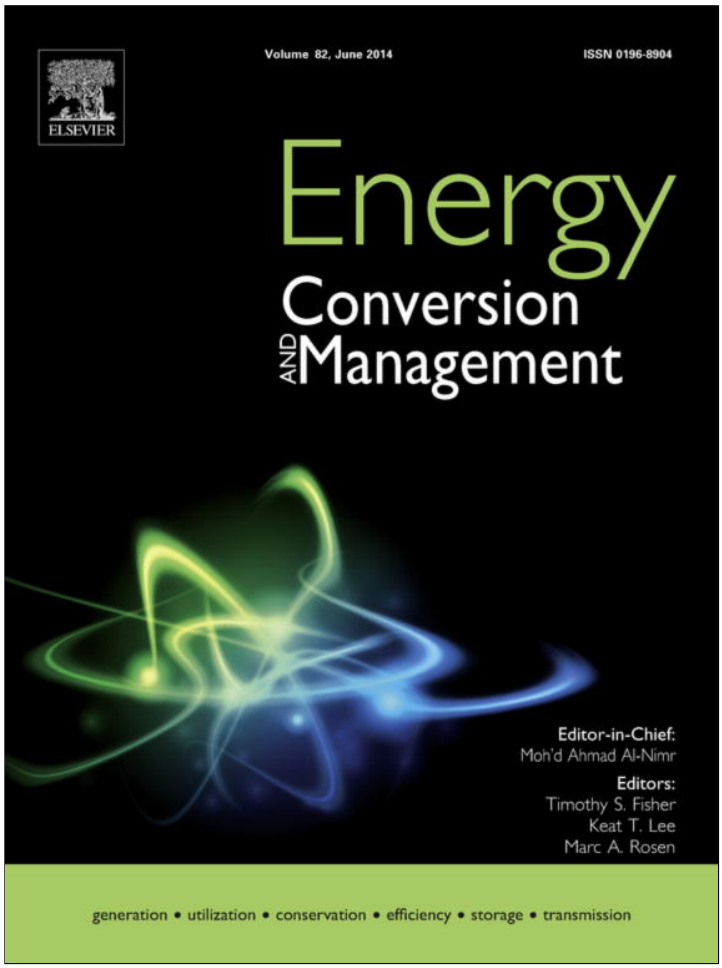

Energy Conversion and Management 82 (2014) 238–243

Contents lists available at ScienceDirect

Energy Conversion and Management

journal homepage: www.elsevier.com/locate/enconman

Structural and optical insights to enhance solar cell performance of CdS nanostructures

Y. Al-Douri [a,*], Q. Khasawneh [b], S. Kiwan [b], U. Hashim [a], S.B. Abd Hamid [c], A.H. Reshak [d,e], A. Bouhemadou [f], M. Ameri [g], R. Khenata [h]

[a] Institute of Nano Electronic Engineering, University Malaysia Perlis, 01000 Kangar, Perlis, Malaysia
[b] Department of Mechanical Engineering, Jordan University of Science and Technology, P.O. Box 3030, Irbid, Jordan
[c] Nanotechnology and Catalysis Research Center (NANOCAT), University of Malaya, 50603 Kuala Lumpur, Malaysia
[d] New Technologies – Research Center, University of West Bohemia, Univerzitni 8, 306 14 Pilsen, Czech Republic
[e] Center of Excellence Geopolymer and Green Technology, School of Material Engineering, University Malaysia Perlis, 01007 Kangar, Perlis, Malaysia
[f] Laboratory for Developing New Materials and their Characterization, Department of Physics, Faculty of Science, University of Setif, 19000 Setif, Algeria
[g] Laboratory Physico-Chemistry of Advanced Materials, University of Djillali Liabes, BP 89, Sidi-Bel-Abbes 22000, Algeria
[h] Laboratoire de Physique Quantique et de Modélisation Mathématique (LPQ3M), Département de Technologie, Université de Mascara, Mascara 29000, Algeria

ARTICLE INFO

Article history:
Received 10 January 2014
Accepted 8 March 2014
Available online 31 March 2014

Keywords:
CdS nanostructures
Spin coating speed
Optical properties

ABSTRACT

Sol–gel spin coating technique is used to prepare nanostructured CdS deposited on glass and quartz substrates with Cd:S 1.2:0.1 mol/L, 1000 rpm spin coating speed at 400 °C and 800 °C annealing temperatures, respectively. The effect of hydrothermal treatment on physical properties of crystalline size and morphology is reported. Structural, topographical and optical properties are investigated using X-ray diffraction (XRD), atomic force microscopy (AFM), UV–visible spectrophotometer (UV) and photoluminescence (PL). The optical properties are investigated experimentally and theoretically to verify the suitable model for electro-optical systems. Our results are in agreement with experimental and theoretical data.

1. Introduction

II–VI semiconductors have transparency properties in the visible range, acoustic characteristics, high electrochemical stability and excellent electronic properties. It has been widely used in chemical sensor [1], surface acoustic wave device [2] and photoanode films of solar cell [3,4]. Different techniques are available to prepare CdS nanostructures including sputtering [5,6], chemical vapor deposition (CVD) [7] and spray pyrolysis [8]. However, among all of these techniques, the sol–gel technique is particularly attractive due to different reasons; good homogeneity, controlled composition, low processing temperature, large area coatings, low cost efficient in producing thin, transparent, multi-component oxide layers of many compositions on various substrates.

Recently, Xu and Yang [9] have used the semiconducting SnS heterojunctions as solar cell structure to study the photovoltaic properties of different SnS heterojunctions, they have researched the CdS/SnS, ZnS/SnS, ZnO/SnS, a-Si/SnS, and SnS/c-Si heterojunctions by numerical analysis and showed that the ZnS/SnS heterojunction has the highest conversion efficiency. They have indicated that the SnS thin film has different roles depending on another material and will affect the window and absorption properties. The less absorption in the window layer and the less photo-generated carrier barrier in the heterojunction interface will lead to the improved photovoltaic properties. While, Tahir and Amin [10] have discussed the recent innovations and potential applications of phototechnology to recycle CO_2 via visible light responsive (VLR) TiO_2-based photocatalyst, in addition to various enhancement methods such as doping with metals and non-metals and sensitization to expand TiO_2 band gap toward visible region. They have presented applications of VLR photocatalysts, advances in photoreactors and future prospects of VLR based technology for conversion of CO_2 to hydrocarbon fuels. The findings revealed both metals and non-metals could improve TiO_2 photoactivity, but non-metals and especially co-metals were more efficient. The combination of co-metals with sensitizers exhibited much higher CO, CH_4 and CH_3OH yield rates. Heidary et al. [11] have elaborated numerically the heat transfer and flow field analysis in anode side of direct methanol fuel cells (DMFCs). They have considered to enhance the heat exchange between bottom cold wall and core flow, bottom wall of fluid delivery channel as corrugated boundary instead of straight (flat) one. Where they have recommended four different shapes of corrugated boundary: rectangular shape,

* Corresponding author. Tel.: +60 4 9798408; fax: +60 4 9798305.
E-mail address: yaldouri@yahoo.com (Y. Al-Douri).

http://dx.doi.org/10.1016/j.enconman.2014.03.020
0196-8904/

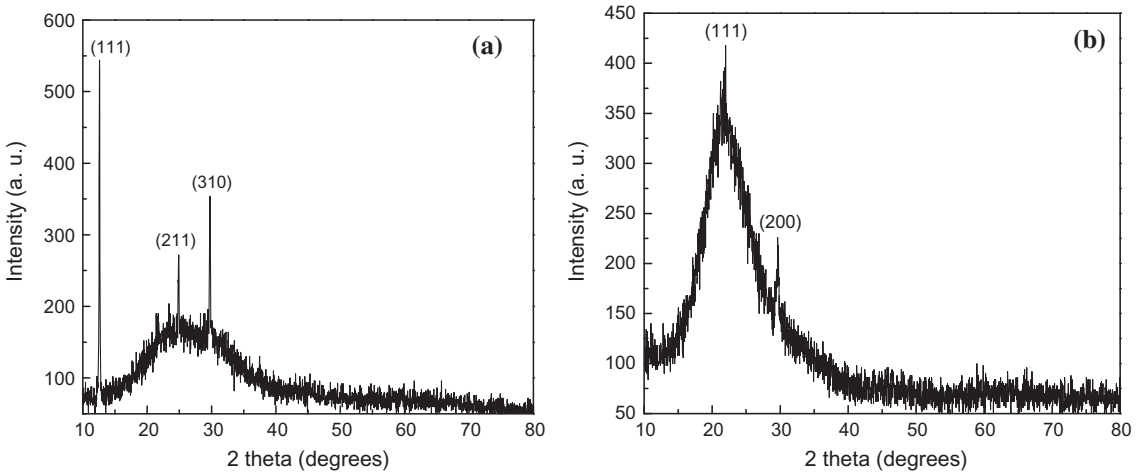

Fig. 1. X-ray diffraction (XRD) patterns deposited on (a) glass substrate annealed at 400 °C and (b) quartz substrate annealed at 800 °C.

Table 1
Grain size, dislocation, strain, interplanar distance and lattice constants deposited on different substrates of nanostructured CdS.

2θ	Substrates	Grain size* (nm)	Dislocation density* (δ) (10^{14} lines/m)	Strain* (ε) (10^{3})	Miller indices* (hkl)	Interplanar distance* (d)	Lattice constants* a and c (Å)
12.58	Glass	4.1206	0.0226	0.0878	111	3.5353	a = 2.354 a = 4.18[a] a = 4.19[b] a = 4.136[c] a = 4.086[d] a = 4.135[e] c = 7.70 c = 6.76[a] c = 6.66[b] c = 6.714[c] c = 6.667[d] c = 6.749[e]
24.88	Glass	2.5739	0.1631	0.1406	211	1.8302	a = 1.218 c = 3.660
29.77	Glass	4.6330	0.2685	0.0781	310	1.5507	a = 1.032 c = 3.101
21.97	Quartz	0.0646	0.1147	5.596	111	2.0581	a = 1.370 c = 4.116
29.62	Quartz	1.3877	0.2649	3.834	200	1.55	a = 1.037 c = 3.115

* Measured value.
[a] Ref. [16] theo.
[b] Ref. [17] theo.
[c] Ref. [18] exp.
[d] Ref. [19] theo.
[e] Ref. [20] exp.

trapezoidal shape, triangular shape and wavy (sinusoidal) shape. The top wall of the channel (catalyst layer boundary) is taken as hot boundary, because reaction occurs in catalyst layer and the bottom wall of the channel is considered as cold boundary due to coolant existence. They have performed a wide spectrum of numerical studies over a range of various shape boundaries, Reynolds number, triangle block number and the triangle block amplitude. With these boundaries, cooling purpose of reacting flow in anode side of DMFCs would be better than straight one. Also, from the analogy between the heat and mass transfer problems, it is expected that the consumption of reacting species within the catalyst layer of DMFCs enhance. They have provided helpful guidelines to the bipolar plate manufacturers of DMFCs to considerably enhance heat transfer and performance of the anode side of DMFC. Theoretically, Al-Douri et al. [12] have calculated the energy band gap using density functional theory (DFT) of the full potential-linearized augmented plane wave (FP-LAPW) method as implemented in WIEN2K code. They used the Engel–Vosko generalized gradient approximation (EV-GGA) formalism to optimize the corresponding potential for energetic transition and optical properties calculations of CdS and CdTe as a function of quantum dot diameter to test the validity of their model of quantum dot potential.

However, this work reports the CdS nanostructures due to its special performance. The characterization, analysis and simulation studies of nanostructured CdS using sol–gel technique are investigated. The classification is as the following; Section 2 displays the experimental process. While, the analysis, characterization and properties studies are presented in Section 3. And Section 4 shows the conclusion.

2. Experimental process

All chemicals were used as received from Sigma–Aldrich Company. CdS nanostructures were grown by sol–gel spin coating technique at room temperature. Polyethylene glycol PEG200 sol was prepared by mixing 0.6 ml of PEG200, 8.5 ml of ethanol and 0.5 ml of acetic acid under stirring for 1 h. 0.1 mol/L of thiourea and 1.2 mol/L of cadmium nitrate as a source of S and Cd, respectively, in addition to 15 ml of ethanol accompanying at 60 °C. Prepared solution was slowly added to PEG200 sol with vigorous stirring for 6 h. As the reaction was started, the reaction system gradually changed from transparent to light yellow. As a preparation case, the solution was ready for deposition using sol–gel technique at 1000 rpm for 30 s. The collected precipitate from centrifugation was dried on hot plate at 120 °C for 1 h and annealed at 400 °C and 800 °C using glass and quartz substrates, respectively for 1 h. The dried and annealed CdS was characterized by atomic force microscopy (AFM), (SII Sciko Instrument INC, SPI 3800N Probe station scan area 2000 nm (2×2 μm) scan speed 2 Hz), and analyzed using X-ray diffraction (XRD), (Philips PW 1710 X-ray diffractometer), UV–visible spectrophotometer, (Perkin Elmer Lambda 950) and Photoluminescence (PL) spectra, (Jobin Yvon Horiba HR800UV system). It was done at room temperature with 325 nm of HeCd laser at 20 mW.

3. Results and discussion

3.1. Analysis and characterization of CdS nanostructures

The nanostructured CdS deposited on different glass and quartz substrates with different annealing temperatures have been

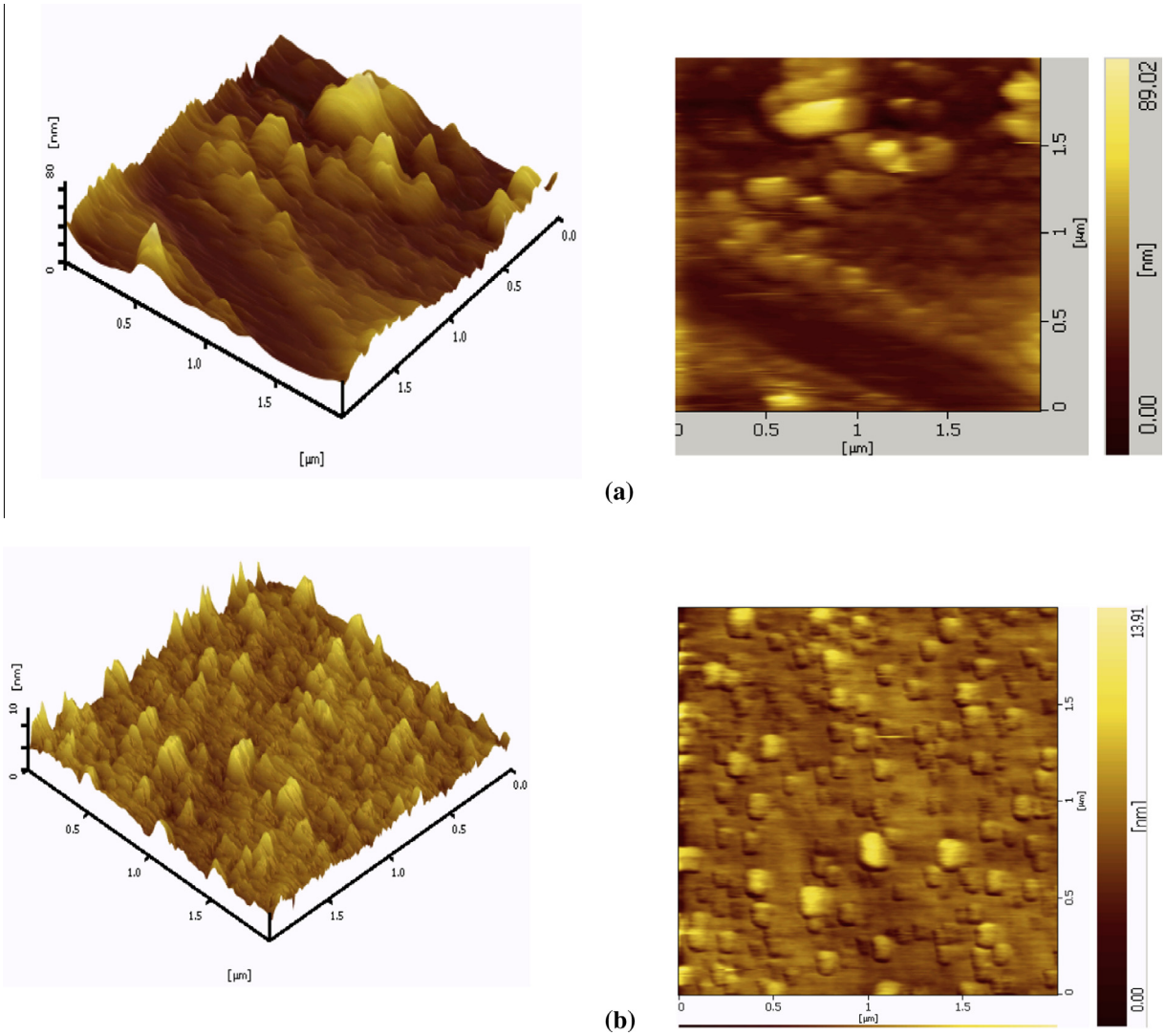

Fig. 2. Atomic force microscopy (AFM) of two and three dimensions deposited on glass and quartz substrates.

investigated by X-ray diffraction (XRD) technique as shown in Fig. 1. It has been prepared at 1000 rpm with cadmium nitrate; 1.2 mol/L and thiourea concentration; 0.1 mol/L. XRD pattern is provided information about crystalline phase of nanoparticles as well as the crystallite size. Fig. 1 shows the XRD pattern of nanostrctured CdS using glass and quartz substrates annealed at 400 °C and 800 °C, respectively. Using glass substrate, the peaks are observed at 12.58°, 24.88° and 29.77° correspond to the (111), (211) and (310) planes, respectively of hexagonal CdS nanostructure. While, using quartz substrate, the peaks are observed at 21.97° and 29.62° correspond to (111) and (200) planes, respectively for hexagonal CdS nanostructure. The intensity of peaks using glass substrate showed higher intensity than using quartz substrate. The observed sharp peak indicates the presence of good crystalline nature, which is good for photocatalytic reaction. Crystallite size (D) was calculated using Scherrer's formula [13,14]:

$$D = 0.91\lambda/\beta\cos\theta \tag{1}$$

where λ is the X-ray wavelength of Cu kα (λ = 1.54 Å), θ is the angle between the incident beam and the reflection lattice planes and β is the full width at half maxima (FWHM) of the diffraction peak in radian. Operating at 35.0 kV, current = 25.0 mA, scan range = 10.000–80.000, scan speed = 5.000 °/min and present time = 0.24 s. The average particle size grown on glass substrate is 4 nm and 1 nm for growing on a quartz one. The defects like dislocation density and strain show inversely correlation [15]. The dislocations are increased gradually contrary to the strains. The dislocation on glass substrate is higher (0.2685×10^{14} liner/m) than on quartz substrate (0.2649×10^{14} lines/m). While, the resulted strain on quartz substrate (5.596×10^{3} unit) is higher than on glass substrate (0.1486×10^{3} unit). In addition, the dislocation density (δ) and strain of the films (ε) were determined using XRD data of the following relations:

$$\delta = 1/D_{hkl}^2 \tag{2}$$

$$\varepsilon = \beta\cos\theta/4 \tag{3}$$

The interplanar distance (d) is calculated using Bragg's formula:

$$d = n\lambda/2\sin\theta \tag{4}$$

while, the lattice constants a and c were calculated using:

$$a = \sqrt{\frac{1}{3}}\lambda \Big/ \sin\theta \tag{5}$$

$$c = \lambda/\sin\theta \tag{6}$$

The structural properties are given in Table 1; they give accordance with other results [16–20]. Further investigation of topography was achieved using atomic force microscope (AFM). The

particles are non-uniformly dispersed. It can be seen from Fig. 2, the 2D and 3D-images of CdS nanostructures deposited on glass substrate with 1000 rpm spin coating speed and annealed at 400 °C, the thickness is 80 nm, while it is 10 nm on quartz substrate at 800 °C as given in Table 2. The conversion efficiency of CdS solar cells is strongly depending on the small roughness of the CdS surface, a reduction of surface roughness tends to increase the conversion efficiency of the solar cells that affect the optical properties as we will see in the subsequent section. However, quartz substrate leads to reduce surface roughness compared to glass substrate. We believe that the conversion efficiency of solar cells can be changed with different substrates and annealing temperatures.

3.2. Optical properties of CdS nanostructures

The optical transmission spectra of the range 200–800 nm are recorded and shown in Fig. 3. The sharp transmission edge of the spectra indicates a good crystallinity of the films. The average transmittance of CdS nanostructure deposited on glass substrate is found to be in the range of 65–70% but on quartz substrate is 80–85%. It can be seen that the transmittance on quartz substrate is higher than on glass one [20,21] due to surface scattering and roughness, thus affecting the %*T* rather that the intrinsic properties of CdS.

The photoluminescence (PL) spectrum is shown in Fig. 4. The synthesized nanoparticles were performed to investigate their luminescence properties. On glass substrate, three emission peaks have been observed that are ascribed to the exciton and trapped luminescence. While, the exciton emission peak appears as sharp band, the trapped emission is broad. CdS nanostructures are deposited on glass substrate exhibit an emission maximum at 397.149 nm (3.13 eV), 527.757 nm (2.35 eV) and 690.205 nm (1.80 eV). While, the CdS nanostructures deposited on quartz substrate exhibit two main emission peaks at 415.344 nm (2.99 eV) and 513.726 nm (2.4161 eV). High-energy band is around 3.13 eV, known as the violet band. A mid-energy band is around 2.35 eV, known as the green band and attributed to interstitial sulfur. A low-energy band, the red band is around 1.80 eV, often attributed to sulfur vacancies [19]. The estimated E_g values for

Table 2
Thickness, energy gap (E_g), refractive index (n) and optical dielectric constant (ε_∞) of CdS nanostructures deposited on glass and quartz substrates using Ravindra et al. [30], Herve and Vandamme [31] and Ghosh et al. [32] models.

Substrates	Annealing temperature* (°C/h)	Cd/S mol/L*	Thickness (t)* (nm)	E_g* (eV)	Refractive index$	Optical dielectric constant$ (ε_∞)
Glass	400/1	1.2/0.1	80	2.35	5.505[f]	30.3050[f]
				2.40[a]	2.5679[g]	6.5941[g]
				2.359[b]	5.3808[h]	28.9530[h]
				2.32[c]	2.52[i]	
				2.42[d]		
				2.361[e]		
Quartz	800/1	1.2/0.1	10	2.4161	5.5459[f]	30.7570[f]
				2.40[a]	2.5431[g]	6.4673[g]
				2.359[b]	5.2936[h]	28.0222[h]
				2.32[c]	2.52[i]	
				2.42[d]		
				2.361[e]		

* Measured value.
$ Calculated value.
[a] Ref. [1] exp.
[b] Ref. [12] theo.
[c] Ref. [21] exp.
[d] Ref. [22] exp.
[e] Ref. [23] theo.
[f] Ref. [30].
[g] Ref. [31].
[h] Ref. [32].
[i] Ref. [20] exp.

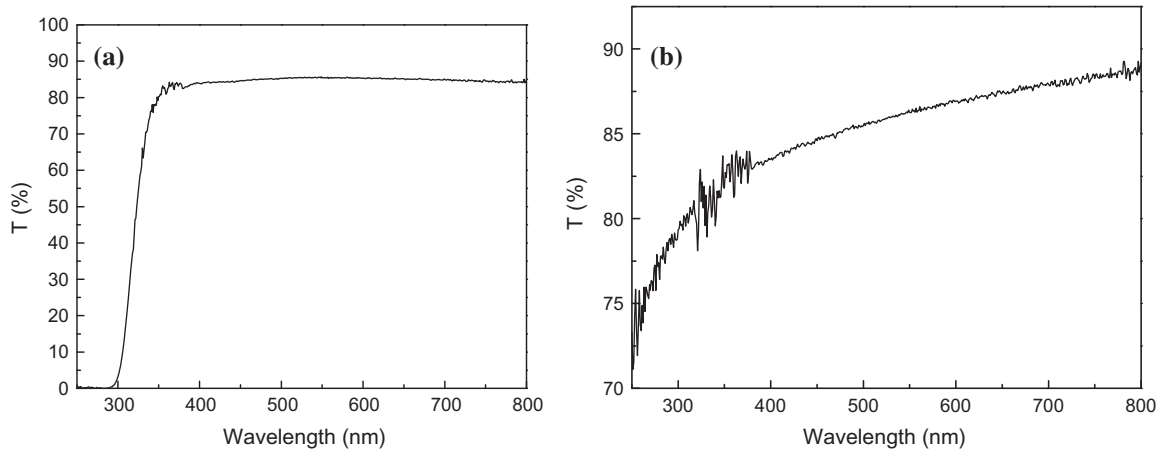

Fig. 3. Transmissions of nanostructured CdS deposited on (a) glass substrate annealed at 400 °C and (b) quartz substrate annealed at 800 °C.

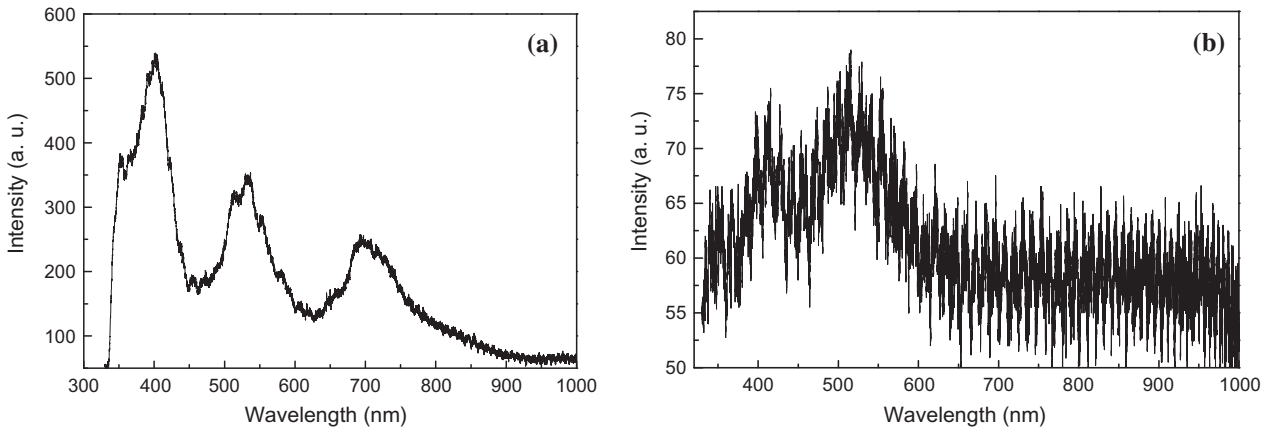

Fig. 4. Photoluminescence (PL) spectroscopy of CdS nanostructure deposited on (a) glass substrate and (b) on quartz substrate.

CdS nanostructures deposited on glass and quartz substrates are given in Table 2. The obtained values give a good agreement with experimental and theoretical results [1,12,21–23].

The refractive index n is an important physical parameter related to microscopic atomic interactions. Theoretically, the two different approaches in viewing this subject are the refractive index related to density, and the local polarizability of these entities [24]. On the other hand, the crystalline structure represented by a delocalized picture, n will be closely related to the energy band structure of the material, complicated quantum mechanical analysis requirements and the obtained results. Many attempts have been made to relate the refractive index n and the energy gap E_g through simple relationships [25–30]. Here, the various relationships between n and E_g will be reviewed to validate the current work. Ravindra et al. [30] had suggested different relationships between the band gap and the high frequency refractive index and presented a linear form of n as a function of E_g:

$$n = \alpha + \beta E_g, \tag{7}$$

where $\alpha = 4.048$ and $\beta = -0.62\ \mathrm{eV}^{-1}$.

To be inspired by simple physics of light refraction and dispersion, Herve and Vandamme [31] had proposed an empirical relation as:

$$n = \sqrt{1 + \left(\frac{A}{E_g + B}\right)^2} \tag{8}$$

where $A = 13.6$ eV and $B = 3.4$ eV. Ghosh et al. [32] had taken a different approach to the problem by considering the band structural and quantum-dielectric formulations of Penn [33] and Van Vechten [34]. Introducing A as the contribution from the valence electrons and B as a constant additive to the lowest band gap E_g, the expression for the high-frequency refractive index are written as:

$$n^2 - 1 = A/(E_g + B)^2, \tag{9}$$

where $A = 25E_g + 212$, $B = 0.21E_g + 4.25$ and $(E_g + B)$ refers to an appropriate average energy gap of the material. Thus, these three models of variation n with energy gap have been calculated. Also, the calculated values of the optical dielectric constant (ε_∞) were obtained using the relation $\varepsilon_\infty = n^2$ [35]. Our calculated refractive index values are in good agreement with experimental value [20] as given in Table 2. This is giving an appropriate model of Herve and Vandamme for solar cells applications.

4. Conclusion

Sol–gel technique is used to characterize and analyze CdS nanostructures deposited on glass and quartz substrates with different annealing temperatures 400–800 °C. It is concluded that the lattice constants measured using XRD patterns are in accordance with experimental and theoretical results. It is found that the average grain size is 4 nm and 1 nm deposited on glass and quartz, respectively. Also, it is found that the transmittance of nanostructured CdS deposited on quartz substrate is higher than the deposited on glass substrate, followed by the measured E_g that is in agreement with experimental and theoretical values. Additionally, the calculated refractive index using Herve and Vandamme model is in agreement with experimental data that recommends the nanostructured CdS deposited on quartz is more appropriate for solar cells applications.

Acknowledgments

Y.A. would like to acknowledge University Malaysia Perlis for grant No. 9007-00062 and TWAS-Italy for the full support of his visit to JUST-Jordan under TWAS-UNESCO Associateship. For the author A.H.R., the result was developed within the CENTEM Project, Reg. No. CZ.1.05/2.1.00/03.0088, co-funded by the ERDF as part of the Ministry of Education, Youth and Sports OP RDI programme. School of Material Engineering, Malaysia University of Perlis, Malaysia. The author (R.K.) acknowledges the support by the National Plan for Science, Technology and Innovation under the research project No. 11-NAN1465-02.

References

[1] Apolinar-Iribe A, Acosta-Enriquez MC, Quevedo-Lopez MA, Ramirez-Bon R, De Leon A, Castillo SJ. Acetylacetone as complexing agent for CdS thin films grow chemical bath deposition. Chalcogenide Lett 2011;8:77–82.
[2] Wacogne B, Roe MP, Pattinson AT. Effective piezoelectric activity of zinc oxide films grown by radiofrequency planar magnetron sputtering. Appl Phys Lett 1995;67:1674–6.
[3] Stolt L, Hedstrom J, Kessler J. ZnO/CdS/CuInSe$_2$ thin-film solar cells with improved performance. Appl Phys Lett 1993;62:597–9.
[4] Keis K, Magnusson Eva, Lindstrom H, Lindquist S-E, Hagfeldt A. A 5% efficient photoelectrochemical solar cell based nanostructured ZnO electrodes. Sol Energy Mater Sol Cells 2002;73:51–8.
[5] Zayer NK, Greerf R, Rogers K, Grellier AJC, Pannell CN. In situ monitoring of sputtered zinc oxide films for piezoelectric transducers. Thin Solid Films 1999;352:179–84.
[6] Nima E. Gorji, Degradation sources of CdTe thin film PV: CdCl$_2$ residue and shunting pinholes. Appl Phys A 2014. http://dx.doi.org/10.1007/s00339-014-8232-7.

[7] Ataev BM, Bagamadova AM, Djabrailov AM. Highly conductive and transparent Ga-doped epitaxial ZnO films on sapphire by CVD. Thin Solid Films 1995;260:19–20.
[8] Joseph B, Gopchandran KG, Thomas PV, Koshy Peter, Vaidyan VK. A study on the chemical spray deposition of zinc oxide thin films and their structural and electrical properties. Mater Chem Phys 1999;58:71–7.
[9] Xu J, Yang Y. Study on the performances of SnS heterojunctions by numerical analysis. Energy Convers Manage 2014;78:260–5.
[10] Tahir M, Amin NS. Advances in visible light responsive titanium oxide-based photocatalysts for CO_2 conversion to hydrocarbon fuels. Energy Convers Manage 2013;76:194–214.
[11] Heidary H, Abbassi A, Kermani MJ. Enhanced heat transfer with corrugated flow channel in anode side of direct methanol fuel cells. Energy Convers Manage 2013;75:748–60.
[12] Al-Douri Y, Baaziz H, Charifi Z, Khenata R, Hashim U, Al-Jassim M. Further optical properties of CdX (X: S, Te) compounds under quantum dot diameter effect: ab initio method. Renew Energy 2012;45:232–6.
[13] Sahraei R, Shahriyar S, Majles MH, Daneshfar AA, Shokri N. Preparation of nanocrystalline CdS thin films by a new chemical bath deposition route for application in solar cells as antireflection coatings. Progress Colorants Coat 2010;3:82–90.
[14] Liu QQ, Shi JH, Li ZQ, Zhang DW, Li XD, Sun Z, et al. Morphological and stoichiometric study of chemical bath deposited CdS films by varying ammonia concentration. Phys B Condens Matter 2010;405:4360–5.
[15] Gorji Nima E. A theoretical approach on the strain-induced dislocation effects in the quantum dot solar cells. Sol Energy 2012;86:935–40.
[16] Knudson MD, Gupta YM, Kunz AB. Time-resolved X-ray diffraction measurements on CdS shocked along the *c* axis. Phys Rev B 1999;59:11704–15.
[17] Madelung O, Scholz M, Weiss H, editors. Numerical data and functional relationships in science and technology. Berlin: Springer-Verlag; 1990.
[18] Wright K, Gale JD. Interatomic potentials for the simulation of the zinc-blende and wurtzite forms of ZnS and CdS: bulk structure, properties, and phase stability. Phys Rev B 2004;70:1–8.
[19] Tan JJ, Li Y, Ji GF. High-pressure phase transitions and thermodynamic behaviors of cadmium sulfide. Acta Phys Pol A 2011;120:501–6.
[20] Weast RC. Handbook of chemistry and physics. 53rd ed. CRC Press; 1972.
[21] Mahdi MA, Kasem SJ, Hassen JJ, Swadi AA, A l-Ani SKJ. Structural and optical properties of chemical deposition CdS thin films. Int J Nanoelectron Mater 2009;2:163–72.
[22] Pan G-T, Shen TF-R, Lai M-H, Juang R-C, Yang C-K. The preparation and characterization of $CdS_{1-x}T_{ex}$ semiconductor films for hydrogen production by the chemical bath deposition method. Sol Energy Mater Sol Cells 2011;95:2524–30.
[23] Feng YP, Teo KL, Li MF, Poon HC, Ong CK, Xia JB. Empirical pseudopotential band-structure calculation for $Zn_{1-x}Cd_xS_ySe_{1-y}$ quaternary alloy. J Appl Phys 1993;74:3948–55.
[24] Balzaretti NM, da Jornad JAH. Pressure dependence of the refractive index of diamond, cubic silicon carbide and cubic boron nitride. Solid State Commun 1996;99:943–8.
[25] Moss TS. A Relationship between the refractive index and the infra-red threshold of sensitivity for photoconductors. Proc Phys Soc Sect B 1950;63:167–76.
[26] Gupta VP, Ravindra NM. Comments on the Moss Formula. Phys Status Solidi (b) 1980;100:715–9.
[27] Al-Douri Y. Electronic and optical properties of $Zn_xCd_{1-x}Se$. Mater Chem Phys 2003;82:49–54.
[28] Al-Douri Y, Feng YP, Huan ACH. Optical investigations using ultra-soft pseudopotential of $Si_{0.5}$ $Ge_{0.5}$. Solid State Commun 2008;148:521–4.
[29] Herve P, Vandamme LKJ. General relation between refractive index and energy gap in semiconductors. Infrared Phys Technol 1994;35:609–15.
[30] Ravindra NM, Auluck S, Srivastava VK. On the Penn gap in semiconductors. Phys Status Solidi (b) 1979;93:k155–60.
[31] Herve PJL, Vandamme LKJ. Empirical temperature dependence of the refractive index of semiconductors. J Appl Phys 1995;77:5476–7.
[32] Ghosh DK, Samanta LK, Bhar GC. A simple model for evaluation of refractive indices of some binary and ternary mixed crystals. Infrared Phys 1984;24:43–7.
[33] Penn DR. Wave-number-dependent dielectric function of semiconductors. Phys Rev 1962;128:2093–7.
[34] Van Vechten JA. Quantum dielectric theory of electronegativity in covalent systems. I. Electronic dielectric constant. Phys Rev 1969;182:891–905.
[35] Samara GA. Temperature and pressure dependences of the dielectric constants of semiconductors. Phys Rev B 1983;27:3494–505.